

Driven polymer translocation in good and bad solvent: effects of hydrodynamics and tension propagation

J. E. Moision,¹ J. Piili,² and R. P. Linna^{2,*}

¹*GE Healthcare, Kuortaneenkatu 2, FI-00510 Helsinki, Finland*

²*Department of Computer Science, Aalto University, P.O. Box 15400, FI-00076 Aalto, Finland*

We investigate the driven polymer translocation through a nanometer-scale pore in the presence and absence of hydrodynamics both in good and bad solvent. We measure tension of the polymer segment on the *cis* side of the pore in the course of translocations simulated using stochastic rotation dynamics, also called multi-particle collision dynamics. We find that in the good solvent the tension propagates similarly whether hydrodynamics is included or not. Only the tensed segment is by a constant factor shorter in the presence of hydrodynamics. The shorter tensed segment and the hydrodynamic interactions contribute to a smaller friction for the translocating polymer when hydrodynamics is included, which shows as smaller waiting times and a smaller exponent in the scaling of the translocation time with the polymer length. Hydrodynamics speeds up translocation in the good solvent, whereas it has a minimal effect on polymer translocation in the bad solvent. Under bad-solvent conditions tension does not spread appreciably along the polymer. Consequently, translocation time does not scale with the polymer length. By measuring the effective friction in a setup where a polymer in free solvent is pulled by a constant force at the end, we find that hydrodynamics does speed up collective polymer motion in the bad solvent even more effectively than in the good solvent. However, hydrodynamics has a negligible effect on the motion of individual monomers within the highly correlated globular conformation on the *cis*-side and hence on the entire driven translocation under bad-solvent conditions.

I. INTRODUCTION

The process of a polymer driven through a nanometer-scale pore by a force acting inside the pore is well understood under good-solvent conditions. It is well established that the polymer is driven out of equilibrium even for moderate pore force. On the *cis* side, that is, on the side from where the polymer translocates, this shows as the tension propagating along the polymer chain [1–5] and on the *trans* side, *i.e.* the side where the polymer translocates to, as crowding of polymer segments [2]. We have previously shown that this crowding has no discernible effect on the driven translocation [5]. The scaling of the translocation time with the polymer length $\tau \sim N^\beta$ in the good solvent follows from the scaling of the length to which the tension has propagated n_t with the number of translocated monomers, or beads, $n_t \sim s^{\beta-1}$. If τ scaled with N also under bad-solvent conditions, tension propagation would be the most likely explaining mechanism.

Hydrodynamics has been shown to speed up driven polymer translocation under good-solvent-conditions [2, 3, 6, 7]. The significance of hydrodynamic interactions under bad-solvent conditions has not been established. As will be seen hydrodynamic interactions is a good way of characterizing how the motion of the polymer segment on the *cis* side takes place.

Previously, we have measured tension propagation along the polymer chain alternatively via the motion of the polymer beads [2] or the strain of individual bonds [5]. Since in the presence of hydrodynamics monomers may be set in motion toward the pore before the tension has reached them, the first-mentioned indirect measurement is not applicable. Encouraged by the very precise measurements of the tension using

the direct method, we will apply it here also in the presence of hydrodynamics. We will determine how fast hydrodynamic interactions set in compared with the speed at which the tension propagates in the good solvent.

The paper is organized as follows: The computational model is explained in Section II. First, the implementation of the polymer and solvent dynamics is covered in subsection A. The polymer model, the indirect implementation of the solvent quality using this polymer model, and the simulation geometry are explained in subsections B, C, and D, respectively. Results are reported and analyzed in Section III. Subsections A and B cover measurements of translocation time and radii of gyration, respectively. The main findings are covered in the subsection C. Here our results from measurements of waiting times, tension, and friction are reported and analyzed. This subsection is further divided in two subsections that cover the results pertinent to the good and bad solvent separately.

II. THE COMPUTATIONAL MODEL

A. Polymer and solvent dynamics

The dynamics of the polymer immersed in the solvent is implemented by a hybrid method where the polymer beads perform molecular dynamics (MD), whose timestep $\delta t = 0.001$, and at every 1000 MD timesteps both the polymer and the solvent perform stochastic rotation dynamics (SRD), whose timestep $\Delta t = 1$. The timesteps along with the distance and potential values that follow are given in reduced units, see *e.g.* [8]. The polymer's equations of motion are integrated in time by the velocity Verlet algorithm [9, 10].

SRD that is used to implement solvent dynamics supports hydrodynamic modes [11]. In the SRD model the simulation space is divided into cubic lattice of cells, whose sides are of unit length. Each cell contains on average 5 solvent particles

* Author to whom correspondence should be addressed: riku.linna@aalto.fi

(SP) and one polymer bead (PB). SPs are fictitious in the sense that they can be thought of as carrying the mass and momenta of multiple realistic particles. The interactions of SPs and PBs are approximated in a stochastic fashion as described below.

An SRD step consists of streaming and collision steps. In the streaming step the position of each solvent particle is propagated according to

$$\mathbf{x}_i(t + \Delta t) = \mathbf{x}_i(t) + \mathbf{v}_i(t)\Delta t. \quad (1)$$

After this the collisions between the solvent particles and the polymer beads are taken into account by

$$\mathbf{v}_i(t + \Delta t) = \mathbf{v}_{\text{COM}}(t) + \mathbf{\Omega}(\mathbf{v}_i(t) - \mathbf{v}_{\text{COM}}(t)), \quad (2)$$

where \mathbf{v}_{COM} is the velocity of the center of mass of the solvent particles and polymer beads within the cell they currently belong to and $\mathbf{\Omega}$ is a stochastic rotation matrix. The rotation angle is constant but the direction of the axis with respect to which the velocities are rotated at each timestep is chosen randomly for each cell. The lattice of cells has periodic boundary conditions.

To maintain molecular chaos, that is, in order to avoid artificial correlations between solvent particles, random grid shifts were applied to the cells before the collision step [12, 13]. In the grid shift the cells (or equivalently the particles) are moved by a displacement between $[-0.5, 0.5]$ of the cell dimension sampled from uniformly random distribution.

A particular advantage of the SRD method is that it allows the switching off of hydrodynamic interactions by randomly shuffling the momenta of the solvent particles after each collision step. This feature is crucial in determining the effects of hydrodynamics on which it is very hard to obtain quantitative information. To pin down the effects of hydrodynamic interactions we will make close comparison between translocation dynamics taking place in a Brownian heat bath and in the presence of full hydrodynamic interactions.

B. Polymer model

In order to gain understanding on the dynamics of polymer translocation under bad solvent conditions we choose a flexible polymer model. The used freely-jointed chain (FJC) model is commonly used to describe single-stranded DNA, RNA, and proteins.

Forces for the equations of motion integrated in time using the velocity Verlet method are obtained from the potentials for the interconnected point-like beads in FJC as $\mathbf{f} = -\nabla V$. Consequent beads in FJC are connected by the anharmonic FENE potential given by

$$V_{\text{FENE}} = -\frac{H}{2}R_0^2 \ln\left(1 - \frac{r^2}{R_0^2}\right), \quad (3)$$

where H is a parameter describing the strength of the potential, r is the distance, and R_0 is the maximum distance between consecutive beads allowed by the FENE constraint. Lennard-Jones potential acts between all PBs

$$V_{\text{LJ}} = 4\epsilon \left[\left(\frac{\sigma}{r}\right)^{12} - \left(\frac{\sigma}{r}\right)^6 \right], \quad r < r_c, \quad (4)$$

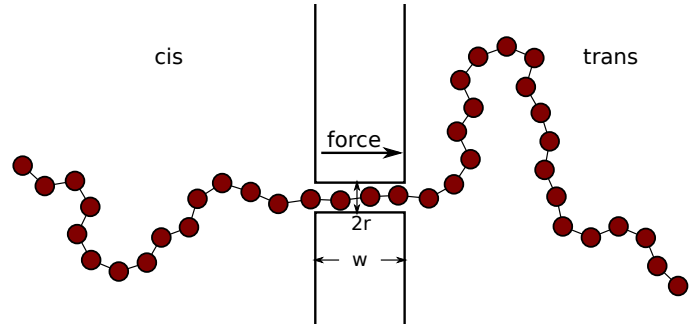


FIG. 1. Schematic depiction of the geometry used in the translocation simulations.

where $\epsilon = 1.2$ is a coupling constant, $\sigma = 1$ sets the length scale of the interactions, and r_c is the cut-off distance for the interaction applied in the case of good solvent (see the next subsection).

C. Implementation of solvent quality

Due to the solvent being implemented by fictitious particles that represent the explicit solvent particles the solvent quality has to be defined indirectly with the aid of monomer interactions. More specifically, LJ potential is used as an effective substitute for real hydrophilic or hydrophobic interactions, since the SRD model for fluid dynamics does not incorporate the complex electrostatic interactions between real solvent and polymer molecules, in contrast to, for example, dissipative particle dynamics (DPD) [14].

A polymer in good solvent can be simulated by truncating the LJ potential at $r_c = 2^{\frac{1}{6}}\sigma$, where $V_{\text{LJ}} = 0$. For a polymer immersed in bad solvent the full form of Eq. (4) that includes the attractive part of the potential is used (*i.e.* $r_c = \infty$). While this indirect implementation has its limitations, causing unphysical artefacts when solvents of two different qualities are used in the same simulation [15], it is valid in any simulation where there is solvent of only one quality present at any time, which is the case in the present study.

D. Translocation geometry and pore model

The translocation geometry is depicted in Fig. 1. The polymer is initially on the *cis* side with three beads inside the pore. An infinite wall parallel to the xy plane divides the simulation space. No-slip boundary conditions bounce the solvent particles and the polymer beads from the wall making it impenetrable for them. The polymer can pass from the *cis* to the *trans* side only through a cylindrical pore, whose axis is parallel to the z axis.

While there is no solvent in the pore, every bead inside the pore experiences a damping force $\mathbf{F}_\gamma = -\gamma\mathbf{v}$, where the damping constant γ is chosen such that the damping inside the pore corresponds to the damping caused by the solvent according to the damping coefficient calculations by Kikuchi

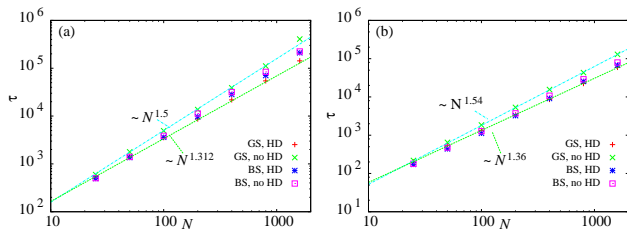


FIG. 2. (Color online) Translocation times τ as a function of polymer length N for good (GS) and bad solvent (BS) with and without hydrodynamics (HD). (a) $F = 1$. (b) $F = 3$.

et al. [16]. A harmonic pore force $\mathbf{F}_h = -k\mathbf{l}$ applied to each bead inside the pore keeps the polymer aligned and prevents hair pinning. Here \mathbf{l} is the displacement vector from pore axis to the bead (perpendicular to the pore axis) and k is a constant.

The translocating polymer is driven by force exerted on the polymer beads inside the pore. The reported driving forces denote the forces applied to each bead inside the pore. Hence, the force applied to the whole polymer is the reported force multiplied by the number of beads inside the pore, which on average is $w/\sigma \approx 3$, where w is the thickness of the wall and σ is the mean distance of the beads. The driving forces considered in this work are in the moderate to large regime ($F\sigma/k_B T \geq 1$) according to the definition by Dubbeldam *et al.* [17].

III. RESULTS

A. Translocation time

Polymers of lengths $N = 25, 50, 100, 200, 400, 800, 1600$ beads were driven through the pore by a force F acting inside the pore. The amount of computation needed for equilibrating the longest chains $N = 800$ and 1600 proved to be extensive. Therefore, the simulations for these polymer lengths were run in parallel using multiple CPU cores. The results were obtained by averaging over at least 200 translocations for chains of length $N \leq 400$ and at least 50 translocations for $N \geq 800$.

As expected, clear scaling of translocation time with the polymer length, $\tau \sim N^\beta$, was obtained for the good solvent case, see Fig. 2. For the large pore force of $F = 10$ stalling events due to local jamming at the pore entrance deteriorate the perfect scaling in the good solvent (not shown). In the good solvent we obtain $\beta \approx 1.5$ and 1.54 for $F = 1, 3$, respectively in the absence of hydrodynamics. The measurements of β for $F = 1$ and 3 not affected by jammings are in accordance with the many times confirmed increase of β with F [2, 5]. We showed that this increase of β with F comes from the *trans* side and addressed it to fluctuations that were shown by Dubbeldam *et al.* to assist translocation [18]. Hydrodynamic interactions decrease β as we have found previously [2]. We obtain $\beta \approx 1.31$ and 1.36 for $F = 1$ and 3 , respectively, when hydrodynamics is included.

In the case of bad solvent the situation is not as clear. τ depends on N in a way where a mechanism resulting in τ scaling with N may play a role, see Fig. 2. However, this mechanism, if there is one, does not dominate the overall translocation dynamics. In simulations made using DPD [14] scaling $\tau \sim N^\beta$ was not obtained for polymer translocation in bad solvent. We will look into this in more detail in the following sections.

In accordance with previous findings [2, 6] hydrodynamic interactions are seen to speed up translocation in good solvent, see Fig. 2. Hydrodynamics does speed up translocation also under bad solvent conditions. However, here the speed-up is small. In the bad solvent where the polymer is in globular conformation tension does not appreciably propagate, as will be seen in Section III C. The increased correlations due to hydrodynamics that enhance momentum transfer along the extended polymer chain in good solvent may not contribute appreciably to the motion of monomers screened by the globular polymer conformation in bad solvent. In addition, it is an open question how effectively hydrodynamics enhances motion in the bad solvent in general. We will determine these issues in Section III C 2.

Regardless of the solvent quality hydrodynamics speeds up the translocation more effectively for large F . The momentum that is mediated along the polymer chain from the pore to the *cis* side is larger for larger F . Drift due to bias dominates over diffusion more strongly for large F . Hence, it is clear that the effect of hydrodynamics via the mediated momentum is more pronounced for large F . The reduction of friction due to hydrodynamics will be dealt with in Section III C.

B. Radius of gyration

Radius of gyration defined as

$$R_g = \sqrt{\frac{1}{N} \sum_{i=1}^N (\mathbf{x}_i - \mathbf{x}_{\text{COM}})^2}, \quad (5)$$

where \mathbf{x}_i and \mathbf{x}_{COM} are the positions of bead i and the center of mass of the polymer, respectively, can be used to determine if a polymer is driven out of equilibrium during translocation [2, 5, 19]. For polymers in equilibrium the relation $R_g^{eq} \propto N^\nu$ holds, where ν is the Flory exponent. We measured $\nu \approx 0.63$ and $\nu \approx 0.31$ for equilibrated polymer conformations in good and bad solvent, respectively.

Fig. 3 shows R_g 's measured during the translocations as a function of the number of beads on the *cis* side $N_{cis} = N - s$ for polymer conformations when hydrodynamics is included. As expected, R_g of the translocating polymers in good solvent show significant deviation from the equilibrium scaling. The polymers in bad solvent maintain their globule equilibrium conformation throughout the translocation process. Small deviation of R_g from the equilibrium scaling can be seen at the end (for small N_{cis}) when the tail of the polymer is sucked into the pore.

Fig. 4 shows R_g measured separately on the *cis* and *trans* sides as a function of the number of translocated beads s for the good solvent together with the plotted $R_g^{eq}(s)$, that is, R_g

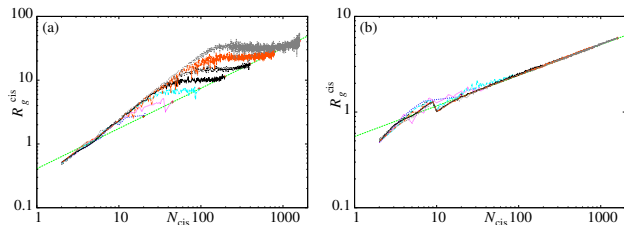


FIG. 3. Measured radii of gyration of the translocating polymers on the *cis* side. The equilibrium R_g measured for seven discrete polymer lengths and the solid line giving the obtained scaling $R_g \sim N^{\nu(\text{measured})}$ are shown for reference. Hydrodynamics is included. $F = 10$. (a) Good solvent, $\nu(\text{measured}) \approx 0.63$. (b) Bad solvent, $\nu(\text{measured}) \approx 0.32$. The chain lengths are (from bottom to top in (a)) $N = 25, 50, 100, 200, 400, 800, 1600$.

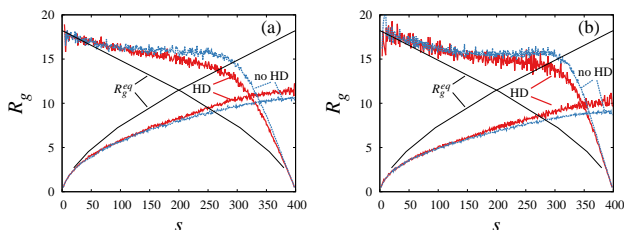


FIG. 4. Good solvent. Measured R_g as a function of the translocation coordinate on the *trans* (plots increasing with s) and *cis* (plots decreasing as s increases) sides. The equilibrium values for the radius of gyration R_g^{eq} are plotted with solid black lines. Hydrodynamics is included, $N = 400$. (a) $F = 1$. (b) $F = 3$.

for equilibrated conformations of s monomers. (For the bad solvent $R_g(s) \approx R_g^{eq}(s)$ for all s and are accordingly not shown.) In accordance with previous findings, R_g deviates increasingly from the equilibrium value R_g^{eq} on both sides in the course of the translocation, see *e.g.* [2]. The measured R_g on both sides deviate more from R_g^{eq} when hydrodynamics is not included. On the *cis* side $R_g > R_g^{eq}$ due to the straightening of the polymer, that is, tension propagation. On the *trans* side $R_g < R_g^{eq}$ due to crowding of monomers.

The crowding results from the polymer exiting the pore faster to the *trans* side than it relaxes to equilibrium. Since the deviation from equilibrium is slightly larger for polymers simulated without hydrodynamics, hydrodynamics speeds up the relaxation of the polymer to thermal equilibrium more than it speeds up translocation. For $F = 10$ the situation changes (not shown). Hydrodynamics speeds up translocation more effectively for larger F . The speed of relaxation to equilibrium does not change with F . Accordingly, the polymer segment on the *trans* side is driven further out of equilibrium for larger F , as seen in Fig. 4. For the very large $F = 10$ (not shown) the polymer conformation on the *trans* side is equally strongly compressed whether hydrodynamics is included or not.

C. Waiting times, tension, and friction

1. Good solvent

It is well established that in good solvent polymer translocation dynamics is in practice determined by the tension propagating along the polymer chain on the *cis* side [1–4, 17, 20, 21]. The mechanism was introduced in [1] and first extracted from simulations by registering the number of moving beads [2]. Recently, we measured tension propagation more accurately and showed that in the absence of hydrodynamics a quasi-static model was sufficient to describe the process with great precision [5]. In the present study we investigate tension propagation when including hydrodynamic interactions.

For reasons that will become evident, in the presence of hydrodynamics the number of moving beads n_d cannot be used as a measure of how far the tension has propagated from the pore to the *cis* side along the polymer chain. The fundamental definition for tension in a bead-spring polymer is the strain measured between all two consecutive beads. The measured values of the bead-to-bead distances turned out to fluctuate strongly and hence require averaging over a vast number of measurements. For this reason, we measure the local straightening of a polymer over three consecutive beads as depicted in Fig. 5. We define the drag distance as $d_i = \|\mathbf{x}_{i+1} - \mathbf{x}_{i-1}\|$. This distance $d_i \approx 2^\nu \sigma$ for polymers in equilibrium and $d_i = 2\sigma$ for a completely straightened polymer segment [5].

d_i for different i are depicted with colors (or with shades of gray in print) as a function of s for polymers in good solvent with and without hydrodynamics for $F = 10$ on the first row of Fig. 6. Tension is seen to propagate qualitatively in the same way in both cases. However, in the presence of hydrodynamics tension propagates slightly less effectively along the chain. This is understandable, since the solvent with hydrodynamic modes mediates the momenta of the moving beads farther from the pore along the chain. Consequently, a bead with a given label n will be set in motion earlier (at a smaller s) in a solvent supporting hydrodynamic modes than in a Brownian heat bath. This results in smaller tension for a given s when hydrodynamics is included.

The first plot on the second row in Fig. 6 shows d_i as a function of s for polymers translocating in a bad solvent that supports hydrodynamics for $F = 10$. As can be seen tension does not propagate appreciably. The plot for the case where polymer translocates in a Brownian heat bath with no hydrodynamics is similar (not shown).

We define the number of beads in the tensed segment n_t on the *cis* side as the number of consequent beads starting from the bead s at the pore for which $d_i > 2^\nu \sigma \approx 1.5$ in the good solvent. In other words, n_t is the difference of the label of the last bead belonging to this segment and the current value of the translocation coordinate s . n_t is the measure of the length of the tensed segment on the *cis* side. For improved resolution we use the threshold value 1.65 for the bond length as a criterion for its end beads to belong to the tensed segment. We denote by the symbol n_d the number of beads in drag, *i.e.* beads that are in motion toward the pore, on the *cis* side. n_d

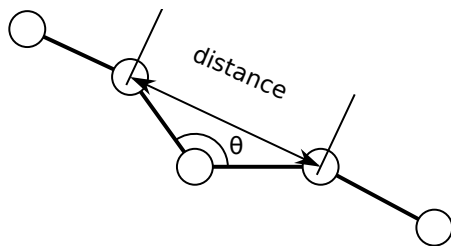


FIG. 5. A schematic five-bead polymer segment showing the measured drag distance over the three middle beads.

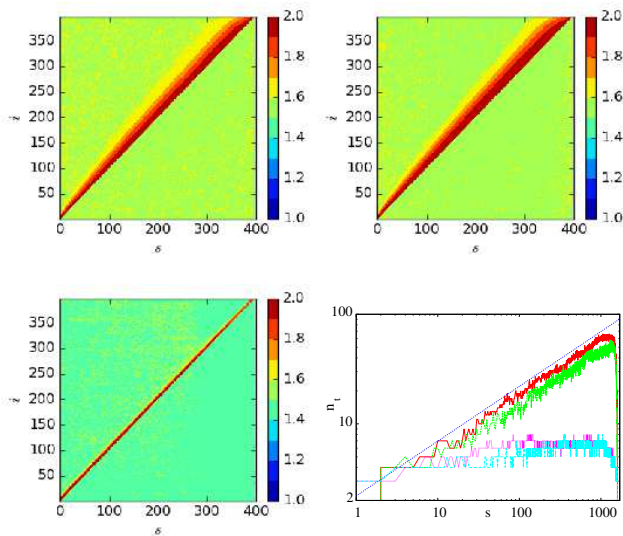


FIG. 6. **The first three figures:** The drag distances d_i of each bead i as a function of the translocation coordinate s . $F = 10$ and $N = 400$. Top left: for good solvent with hydrodynamics. Top right: for good solvent without hydrodynamics. Bottom left: for bad solvent with hydrodynamics. **The last figure:** A logarithmic plot of the number of beads in the tensed segment n_t on the *cis* side as a function of s . $F = 3$ and $N = 1600$. Curves from top to bottom: Good solvent without hydrodynamics, good solvent with hydrodynamics, bad solvent without hydrodynamics, and bad solvent with hydrodynamics. The dotted line shows the scaling $\sim s^{0.5}$.

that differs somewhat from n_t , especially when hydrodynamics is included, is not measured here but used to denote the actually moving polymer segment that determines the friction on the *cis* side.

The last plot in Fig. 6 shows n_t as a function of s for $F = 3$. The tension is seen to spread more effectively in the absence of hydrodynamic interactions even in the case of bad solvent where tension spreading is negligible. From this logarithmic plot it is also evident that the spreading tension gives the resultant scaling of the translocation time $\tau \sim N^\beta$ under good solvent conditions.

The waiting time $t_w(s)$ is defined as the time required for the bead s to reach the pore after the instant when the bead $s - 1$ has entered the pore. In Figs. 7 (a)-(c) the number of beads in the tensed segment $n_t(s)$ and waiting times $t_w(s)$ are compared for the translocation in good solvent driven by

$F = 3$. In the absence of hydrodynamic interactions, see Fig. 7 (a), $n_t(s)$ depends on s in almost exactly the same way as t_w , that is, $n_t(s) \propto t_w(s)$, which is in agreement with the results from our previous study using Langevin dynamics. In this study we showed that a quasi-static model, where the tension spreading is described only geometrically and for example inertia of the beads set in motion is ignored describes the process fairly accurately [5].

The relation $t_w \propto n_t$ in a good solvent without hydrodynamics is a consequence of the driven translocation taking place strongly out of equilibrium [2]. Hence, the process can be largely described by how the frictional force η changes on the *cis* side. In the quasi-static model [5] the beads from s to $s + n_t$ are considered to be the only non-stationary beads affecting the translocation dynamics, the other beads being at rest. The driving force must balance the friction experienced by n_d beads moving with velocity v towards the pore $F = \eta = n_d \gamma v$, or $v^{-1} \propto n_d$. Hence, when the bead $s - 1$ is at the pore, the time required for the next bead s to reach the pore is given by $t_w(s) \approx \sigma/v(s) \propto n_d(s) = n_t(s)$. The last equality holds in the absence of hydrodynamics. The translocation time $\tau = \int_0^{N-1} t_w(s) ds$. Accordingly, if $n_t(s) \sim s^\xi$ in the tension propagation phase, then disregarding the final retraction of the polymer tail $\tau \sim N^\beta$, where $\beta = \xi + 1$. From the last plot in Fig. 6 we can read $\beta \approx 1.5$.

Hydrodynamic interactions break the relation $t_w \propto n_t$, as seen in Fig. 7 (b). The friction increasing with n_t is still a determining factor for the waiting time profile $t_w(s)$. However, due to the backflow beads start moving before tension reaches them. The backflow of the moving beads sets beads in motion farther from the pore than where the tension has propagated. This leads to smaller n_t in the presence of hydrodynamics. Consequently, $n_t < n_d$ when hydrodynamics is included. Also, in contrast to the translocation dynamics in the Brownian heat bath, the friction is not directly proportional to n_d when hydrodynamics is included but determined by the hydrodynamic radius of the moving polymer segment.

In Fig. 7 (b) n_t and t_w are compared with and without hydrodynamics. $t_w(s)$ is seen to initially increase as rapidly in the presence and absence of hydrodynamics. It takes a while for the hydrodynamic modes to fully develop after the first polymer beads are set in motion. Before this the translocating polymers immersed in solvents with and without hydrodynamics experience identical friction. After this setting-in time for hydrodynamics the friction for the translocating polymer in the solvent with hydrodynamics is much smaller. Consequently, the $t_w(s)$ profile grows more weakly with s than the $n_t(s)$ profile. This is also clearly seen in the logarithmic plots of $n_t(s)$ and $t_w(s)$ in Fig. 7 (c). $n_t(s)$ scale identically for the cases with and without hydrodynamics. In the absence of hydrodynamics $t_w(s)$ is closely aligned with $n_t(s)$, whereas $t_w(s)$ scales with s with a clearly smaller exponent than $n_t(s)$ when hydrodynamics is included.

During the translocation the waiting time t_w increases to a maximum before dropping rapidly due to the final retraction of the remaining polymer segment on the *cis* side. The ratio for the waiting times in the absence and presence of hydrodynamics $R = t_w^{noHD}(s)/t_w^{HD}(s)$ reaches a maximum R_{max} at

this same point. For $N \leq 800$, R_{max} does not change with F but increases with N . We obtain $R_{max} = 1.2, 1.3, 1.5, 1.7, 2$, and 2 for $N = 25, 50, 100, 200, 400$, and 800 . This characteristic is explained by tension not having a sufficient time to evolve before retraction starts for short polymers, as seen from Fig. 7 (d) showing $n_t(s/N)$ for different N in the absence of hydrodynamics. Consequently, the tension profiles in the absence and presence of hydrodynamics differ less for short polymers.

Only for $N = 1600$ values of R_{max} differ slightly for different F ; namely $R_{max} = 3$ for $F = 1$ and $R_{max} = 2.3$ for $F = 3$ and 10 . As seen in Fig. 7 (d), translocation of the polymer of length $N = 1600$ is occasionally stalled already for $F = 3$. This stalling affects not only R_{max} but also β , for $F = 10$.

In Fig. 8 we look more closely at the lengths of the tensed segments. n_t increases with pore force F , see Fig. 8 (a). In other words, tension propagates faster for larger driving pore force. It is noteworthy that the tension propagates farther for larger F in spite of the fact that also the polymer translocates faster and so spends less time on the *cis* side. Hence, increasing F speeds up tension propagation more than polymer translocation.

For $F = 1$ and $F = 3$ tension propagates more strongly in the absence of hydrodynamic interactions. The difference in tension propagation for the cases with and without hydrodynamics is largest for small F and decreases when increasing F until it disappears for $F = 10$, where tension propagates so fast that it overrides the effect of the hydrodynamic backflow, whose effect is seen for $F = 1$ and 3 .

Although the magnitudes of $n_t(s)$ with and without hydrodynamics are different the shapes are identical, which can be seen in Fig. 8 (b), where the tension profiles $n_t(s)$ for $F = 1$ and 3 with hydrodynamics are scaled to make them align with the corresponding $n_t(s)$ without hydrodynamics. In other words, tension propagates along the polymer chain on the *cis* side similarly during the translocation for the cases with and without hydrodynamics. Only the magnitudes of $n_t(s)$ are smaller when hydrodynamics is involved for $F < 10$. The length of the tensed segment without hydrodynamics is by the factor $A = 1.5$ larger than with hydrodynamics for $F = 1$. For $F = 3$ $A = 1.1$. For $F = 10$ tension profiles for translocations with and without hydrodynamics are identical ($A \approx 1.0$).

The increase of n_t with increasing F gets weaker for larger F . This is what is expected from the inertial contribution. When a bead at the end of the tensed segment is being pulled by a moderate force, the next bonded bead starts moving in the viscous heat bath before the bond (or spring) is fully stretched. As the force increases the bond gets increasingly extended before the next bead starts moving. For a sufficiently large force the bond gets fully extended before the next bead moves. For such a large force inertial effects play no role. This corresponds to the quasi-static model [5]. n_t cannot increase beyond the extent given by the quasi-static model and by increasing F we will approach this model where beads that are set in motion from their initial positions start immediately moving at the velocity of the pulling bead.

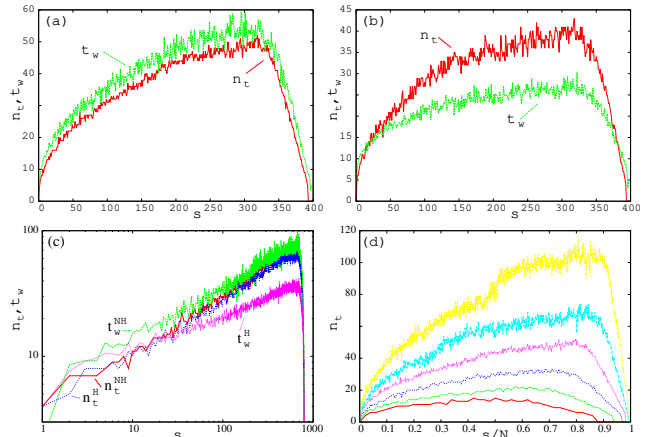


FIG. 7. Comparison of the number of beads in the tensed segment n_t and the waiting times t_w as a function of the translocation coordinate s in the good solvent. $F = 3$. (a) Hydrodynamics not included. $N = 400$. (b) Hydrodynamics included. $N = 400$. (c) Logarithmic plots of $n_t(s)$ and $t_w(s)$ with (H) and without hydrodynamics (NH). $N = 800$. (d) n_t as a function of the normalized reaction coordinate s/N with no hydrodynamics, $F = 3$. From bottom to top $N = 50, 100, 200, 400, 800$, and 1600 .

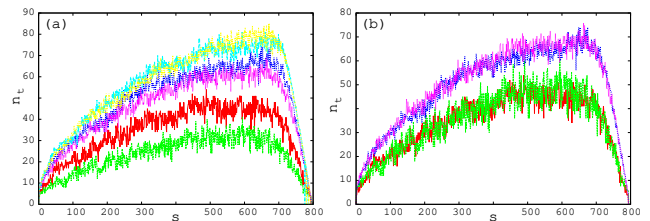


FIG. 8. Good solvent, $N = 800$. (a) The length of the tensed segment on the *cis* side during translocation $n_t(s)$. Curves from bottom to top: (i) $F = 1$, with hydrodynamics (HD), (ii) $F = 1$, no HD, (iii) $F = 3$ with HD, (iv) $F = 3$ no HD, (v & vi) $F = 10$ with and without HD. (b) Tension profiles $n_t(s)$ with and without HD. $n_t(s)$ with HD are scaled, $An_t(s)$, such that perfect alignment with no-HD-profiles are obtained. $A = 1.5$ for $F = 1$ (lower curves) and $A = 1.1$ and $F = 3$ (upper curves).

These inertial effects contribute to a dependence established in a number of studies, namely that the translocation time is not strictly inversely proportional to the driving force, but instead $\tau \sim F^{-\alpha}$, where $\alpha < 1$. In a previous study we obtained $\alpha \approx 0.94$ and 0.99 with and without hydrodynamics, respectively [2]. Here, we obtain $\alpha \in [0.8, 0.9]$. The range of F here is not sufficiently wide to extract precise values for α . We also note that the pore details affect α . A narrower pore gives a smaller α . The pore diameter in the present study is 0.5 whereas in our study cited above it was 0.6 . Qualitatively the same tendency was obtained here: α is smaller when hydrodynamics is included.

In order to have some idea of the relative importance of the two factors contributing to the speed-up due to hydrodynamics, namely the backflow and the reduction of friction, we performed simulations where a polymer in free solvent (no walls, periodic boundaries) is pulled at the end by constant force

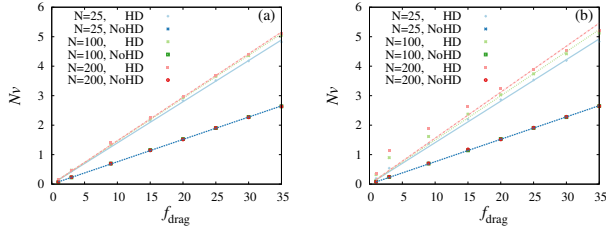


FIG. 9. Terminal velocity times polymer length Nv as a function of dragging force f_{drag} for polymers of different lengths. (a) Good solvent. (b) Bad solvent.

TABLE I. The constants C of Eq. (6) for polymers of different length N with and without hydrodynamics (HD) and their ratios. Good (GS) and bad solvent (BS).

N	$C_{\text{HD}}^{\text{GS}}$	$C_{\text{noHD}}^{\text{GS}}$	$C_{\text{HD}}^{\text{GS}}/C_{\text{noHD}}^{\text{GS}}$	$C_{\text{HD}}^{\text{BS}}$	$C_{\text{noHD}}^{\text{BS}}$	$C_{\text{HD}}^{\text{GS}}/C_{\text{noHD}}^{\text{BS}}$
1	0.0735	0.0731	1.01	0.0735	0.0731	1.01
25	0.140	0.0758	1.84	0.141	0.0760	1.85
100	0.146	0.0759	1.92	0.150	0.0760	1.97
200	0.147	0.0757	1.95	0.156	0.0762	2.05
400	0.148	0.0755	1.96	-	-	-

f_{drag} . These simulations were started from straight polymer conformations that are relatively close to the quasi-static conformations that the polymers assume after being dragged for a sufficiently long time. We checked that similar conformations (and terminal velocities) were obtained by starting from equilibrated conformations. The velocity of the polymer was measured after it had reached the terminal value, as we have previously done for sedimenting polymers [22]. The measurement was done for polymers of different lengths and for different f_{drag} (10 runs per parameter pair).

The measured components of the terminal velocities parallel to f_{drag} follow quite accurately the relation

$$v = C_{(\text{HD}/\text{noHD})} \frac{f_{\text{drag}}}{N}, \quad (6)$$

where the constants $C_{\text{HD}} \approx 0.15$ and $C_{\text{noHD}} = 0.076$ are for the cases with and without hydrodynamics, respectively. In Fig. 9 (a) the terminal velocities multiplied by the polymer lengths are plotted as a function of f_{drag} . The values for the coefficients are given in Table I. Hydrodynamics is seen to speed up the motion of the dragged polymers of lengths $N \in [25, 400]$ by a factor $C_{\text{HD}}/C_{\text{noHD}} \approx 1.9$. Since the effect of backflow is insignificant in the case of a fully extended polymer being pulled at the end, this is the ratio of the frictions in the absence and presence of hydrodynamics. From Fig. 7 (d) and comparing $C_{\text{HD}}/C_{\text{noHD}}$ to the maximum ratio of waiting times R_{max} above hydrodynamic modes can be estimated to have time to develop fully before retraction for polymers of length $N \geq 400$. The backflow plays a role at the initial and intermediate stages of translocation, but before the retraction at the end of the tension propagation the driven polymer translocation for a realistic pore bias has reached a state where hydrodynamics speeds up the motion solely due to the reduced friction.

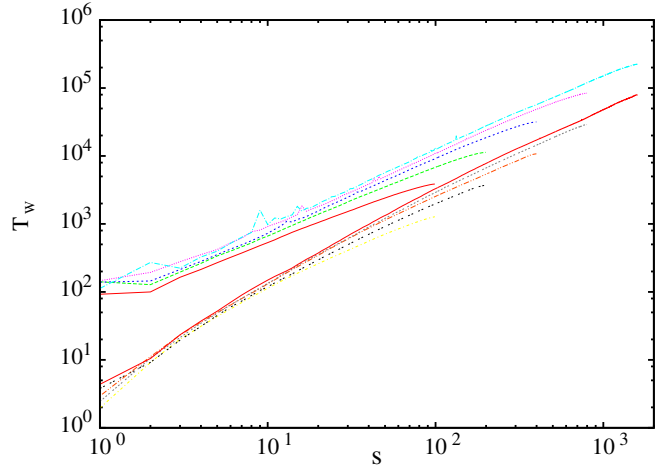


FIG. 10. Translocation in bad solvent, no hydrodynamics. Logarithmic plot of cumulative waiting times $T_w(s)$ for $F = 1$ (upper curves) and 3 (lower curves). Polymer lengths $N = 100, 200, 400, 800,$ and 1600.

2. Bad solvent

In the bad solvent tension does not appreciably propagate along the polymer chain on the *cis* side, in contrast to the translocation in good solvent, see Figs. 3 and 6. Accordingly, there is no scaling of τ with N due to tension propagation. This is clearly seen in Fig. 10 showing cumulative waiting times $T_w(s) = \int_0^s t_w(s') ds'$ for $F = 1$ and 3 and $N \in [100, 1600]$.

Right from the beginning of translocation the waiting times are seen to be larger for longer chains. This reflects the correlated motion of the polymer beads in the globular (and entangled) conformation in the bad solvent. Unlike in the good solvent the correlation length in the bad solvent extends over the whole polymer segment on the *cis* side. Hence, a single moving monomer having to push other monomers out of its path experiences a friction that increases with the number of monomers on the *cis* side. The waiting times increasing for all s when increasing N is in stark contrast with waiting times of translocations in good solvent that for polymers of different N are aligned up to the value of s , where the final retraction from the *cis* side starts. Consequently, in the bad solvent the waiting time profile does not result in the scaling of τ with N like in the good solvent. There is, however, a linearly growing part in $T_w(s)$ when $s \rightarrow N$.

Fig. 9 (b) shows the terminal velocity times the polymer length Nv as function of f_{drag} in the case of bad solvent for $N = 25, 100,$ and 200 when a polymer is pulled in free solvent by a constant force f_{drag} at the end. As was the case in the good solvent, the polymers start from a straight conformation. For strong f_{drag} the conformations remain fairly straight but for weak f_{drag} polymers have a globular portion. In the absence of hydrodynamics individual monomers experience a similar friction regardless of the length of the pulled polymer. This is seen as a collapse of Nv curves for polymers of

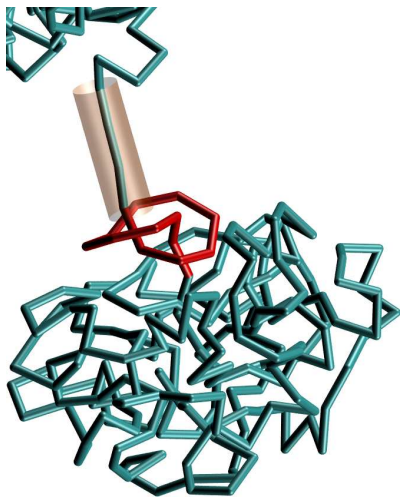


FIG. 11. A snapshot of a simulation with bad solvent at the reaction coordinate value $s = 1400$. A trefoil knot (emphasized in red) is seen at the pore entrance. $N = 1600$ and $F = 3$. For improved visibility the polymer is depicted with a tube of diameter 0.2 that is smaller than the diameter of 1 implied by the Lennard-Jones interaction range.

different N .

In the presence of hydrodynamics individual monomers belonging to longer polymers obtain higher velocities than those belonging to shorter ones. Also, polymers pulled by a constant force obtain higher velocities in a bad than in a good solvent. Both these features are due to the backflow assisting a polymer with a prominent globular part. The effect of the backflow is not significant for the straight polymers in the good solvent. The coefficients in Eq. (6) for the bad-solvent case are shown in the three rightmost columns of Table I.

In spite of hydrodynamics assisting collective motion of a globular polymer segment in the pulling experiment, it has a negligible effect on driven translocation in the bad solvent. In the case of translocation individual monomers that are pulled toward the pore are surrounded by immobile monomers, so that long-ranged hydrodynamic modes in the direction of the motion do not form. Accordingly, although hydrodynamics speeds up collective center-of mass motion of entire polymer conformations even more effectively in the bad than in the good solvent, it has a negligible effect on the driven translocation in the bad solvent.

It is also noteworthy that for polymers of realistic lengths knots slow down translocation. In our simulations stalling effects in individual translocations due to knots are seen for polymers of lengths $N = 800$ and 1600 . Fig. 11 shows a snapshot of a simulated translocation where a trefoil knot is at the pore entrance.

IV. SUMMARY

We have studied driven polymer translocation in the good and the bad solvent in the presence and absence of hydrodynamic modes using stochastic rotation dynamics coupled with

molecular dynamics. By measuring the radii of gyration R_g on both sides of the pore we found that during the translocation polymers were driven out of equilibrium only in the good solvent. The mechanisms to this effect are well established, namely tension propagation on the *cis* and monomer crowding on the *trans* side. In the bad solvent polymer translocated through the pore practically from one equilibrium conformation to another. Here, translocations driven by large pore force magnitudes were seen to be occasionally stalled by knots present already in the initial random conformations.

In the good solvent the *trans* side polymer conformations deviated from equilibrium conformations less when hydrodynamics was included. This means that hydrodynamics speeds up polymer's relaxation toward equilibrium even more than it speeds up its translocation. Also on the *cis* side R_g of the polymer conformations deviate less from the equilibrium values when hydrodynamics is involved. This is a manifestation of the backflow setting monomers in motion before the tension propagating from the pore has reached them. Consequently, the polymer is less tensed, or less extended, on the *cis* side in the presence of hydrodynamics.

Tension measurements showed that in the beginning of the translocation tension propagates along the polymer chain on the *cis* side identically in the presence and absence of hydrodynamics. This is due to the set-in time required for the hydrodynamic modes to fully develop. After this initial stage the friction is smaller when hydrodynamics is included, as expected. Consequently, the waiting time that is to a good precision proportional to the friction scales with the number of translocated monomers with a smaller exponent in the presence of hydrodynamics. In other words, a smaller scaling exponent is obtained for the translocation time τ with the polymer length N in the presence of hydrodynamics. The scaling for asymptotically long polymers is expected to be the same, $\tau \sim N^{1+\nu}$, where ν is the Flory exponent, both in the absence and presence of hydrodynamics.

It is noteworthy that although the waiting time increases with the number of translocated monomers by a smaller exponent when hydrodynamics is included, the length of the tensed segment increases with the same exponent. In other words, tension propagates qualitatively in the identical manner whether hydrodynamics is included or not. Only the length magnitude of the tensed segment at all stages is smaller due to backflow when hydrodynamics is included.

In the bad solvent the tension does not propagate appreciably on the *cis* side. Accordingly, the translocation time does not show a clear scaling with the polymer length in the bad solvent. The waiting times at the initial stages of the translocations are longer for longer polymers, which is due to the increased friction that the moving monomers experience by the relatively immobile monomers in their path within the globular conformations. However, for very long polymers translocation time seems to approach linear dependence on the polymer length.

By measuring terminal velocities for polymers in free solvent pulled at the end, we could determine the speed-up due to hydrodynamics in the good solvent to result almost entirely from the reduced friction and to a lesser extent from the back-

flow. Surprisingly, hydrodynamics was seen to speed up the pulled polymer in the bad solvent more than in the good solvent. In addition, the motion of longer polymers was sped up more than the motion of short polymers. In the pulling experiment the globular polymer conformation moves 'as a whole', that is, by collective center-of-mass motion of the monomers in contrast to translocation where individual monomers move within the globular conformation. The backflow has a much stronger effect on the motion of a globular than a stretched polymer. Hence, in the presence of hydrodynamics the pulled polymers move faster in the bad than in the good solvent and the longer polymers with a sufficiently large globular part move faster than short polymers.

To recap, there is no tension propagation nor the accompanying scaling of the translocation time τ with the polymer length N in the driven translocation in the bad solvent. Hydrodynamics that speeds up translocation in the good solvent

and decreases the scaling exponent β in the good solvent has only a negligible effect in the bad solvent. In the biological context the polymer translocation takes place in solutions abundant with biological organelles, which can make the solvent quality effectively bad. Hence, the scaling characteristics obtained for the generic translocation in the good solvent may not be completely valid for the *in vivo* translocation processes.

ACKNOWLEDGMENTS

Mr. Pauli Suhonen is acknowledged for his contribution in the useful discussions. The computational resources of CSC-IT Centre for Science, Finland, and Aalto Science-IT project are acknowledged. The work of Joonas Piili is supported by The Emil Aaltonen Foundation and The Finnish Foundation For Technology Promotion.

-
- [1] T. Sakaue, *Physical Review E* **76**, 021803 (2007).
 [2] V. V. Lehtola, R. P. Linna, and K. Kaski, *Europhysics Letters* **85**, 58006 (2009).
 [3] V. V. Lehtola, R. P. Linna, and K. Kaski, *Physical Review E* **78**, 061803 (2008).
 [4] T. Ikonen, A. Bhattacharya, T. Ala-Nissila, and W. Sung, *Physical Review E* **85**, 051803 (2012).
 [5] P. M. Suhonen, K. Kaski, and R. P. Linna, *Phys. Rev. E* **90**, 042702 (2014).
 [6] M. G. Fyta, S. Melchionna, E. Kaxiras, and S. Succi, *Multi-scale Modelling & Simulation* **5**, 1156 (2006).
 [7] S. Melchionna, M. Fyta, E. Kaxiras, and S. Succi, *International Journal of Modern Physics C* **18**, 685 (2007).
 [8] M. P. Allen and D. J. Tildesley, *Computer Simulation of Liquids* (Clarendon Press, Oxford, 2006).
 [9] W. C. Swope, H. C. Andersen, P. H. Berens, and K. R. Wilson, *The Journal of Chemical Physics* **76**, 637 (1982).
 [10] D. Frenkel and B. Smit, *Understanding Molecular Simulation*, 2nd ed. (Academic Press, 2002).
 [11] A. Malevanets and R. Kapral, *Journal of Chemical Physics* **110**, 8605 (1999).
 [12] T. Ihle and D. M. Kroll, *Physical Review E* **63**, 020201 (2001).
 [13] T. Ihle and D. M. Kroll, *Physical Review E* **67**, 066705 (2003).
 [14] K. Yang, V. A., and A. V. Neimark, *The Journal of Physical Chemistry B* **117**, 3648 (2013).
 [15] F. Kapahnke, U. Schmidt, D. W. Heermann, and M. Weiss, *Journal of Chemical Physics* **132**, 164904 (2010).
 [16] N. Kikuchi, C. M. Pooley, J. F. Ryder, and Y. J. M., *Journal of Chemical Physics* **119**, 6388 (2003).
 [17] J. L. A. Dubbeldam, V. G. Rostiashvili, A. Milchev, and T. A. Vilgis, *Physical Review E* **85**, 041801 (2012).
 [18] J. L. A. Dubbeldam, V. G. Rostiashvili, A. Milchev, and T. A. Vilgis, *Phys. Rev. E* **87**, 032147 (2013).
 [19] A. Bhattacharya and K. Binder, *Phys. Rev. E* **81**, 041804 (2010).
 [20] T. Sakaue, *Physical Review E* **81**, 041808 (2010).
 [21] P. Rowghanian and Y. A. Grosberg, *Journal of Physical Chemistry B* **115**, 14127 (2011).
 [22] J. Piili, D. Marenduzzo, K. Kaski, and R. P. Linna, *Phys. Rev. E* **87**, 012728 (2013).